energies

MDPI

Article

Concentration of CO_2 in the Local Working Area during the Joint Operation of a Gas Infrared Heater and an Air-Exchange System

Boris Vladimirovich Borisov, Geniy Vladimirovich Kuznetsov, Vyacheslav Ivanovich Maksimov *, Tatiana Aleksandrovna Nagornova and Felix Yurievich Salikhov

School of Energy and Power Engineering, National Research Tomsk Polytechnic University, 634050 Tomsk, Russia
* Correspondence: elf@tpu.ru

Abstract: The formation of local areas in large buildings with regulated thermal conditions is an urgent task. The use of gas infrared heaters for this purpose raises questions on the utility of an air-exchange system and the monitoring of the combustion product concentration. In this study, the modeling of heat transfer processes on premises with a gas infrared heater and an air-exchange system was conducted. The carbon dioxide concentration in the local working area when using a light-type gas infrared heater was determined. The regularities of current formation for circulating air and combustion products on the premises at various air-exchange rates were analyzed. The profiles of CO_2 temperatures and concentrations in the local working areas on the left and right of the equipment model are shown. The article makes a conclusion about the influence of air velocity from the air-exchange system based on average values of carbon dioxide concentration on the premises and in the local working area. The possibility of increasing the temperature in the local working area without exceeding the permissible CO_2 concentrations (less than 1000 ppm) has been identified. The formulated approach allows us to predict the available modes of the air-exchange system to create the highest possible comfort heating parameters while maintaining an acceptable degree of air pollution from combustion products.

Keywords: gas infrared heater; air-exchange system; local working areas; fields of temperatures; field CO_2 concentrations

Citation: Borisov, B.V.; Kuznetsov, G.V.; Maksimov, V.I.; Nagornova, T.A.; Salikhov, F.Y. Concentration of CO_2 in the Local Working Area during the Joint Operation of a Gas Infrared Heater and an Air-Exchange System. *Energies* **2024**, *17*, 155. https://doi.org/10.3390/en17010155

Academic Editor: Ioan Sarbu

Received: 17 November 2023
Revised: 14 December 2023
Accepted: 21 December 2023
Published: 27 December 2023

1. Introduction

The use of gas infrared heaters (GIHs) has a number of advantages over traditional heating systems [1,2]. One of the main benefits lies in the possibility of creating local thermal areas in large industrial premises [3–5]. The creation of such areas is most expedient with the help of light-type GIHs [4,6]. They have a higher power (compared to dark-type ones [4,6]), which is reached through open gas combustion. However, such combustion leads to combustion product emissions (mainly CO_2) into the environment. For this reason, the air-exchange system's operation is required during light-type GIH use [7–9]. When creating thermal areas for a worker, it is advisable to maintain regulated thermal conditions (microclimate) [10–13]. Therefore, parameters such as temperature, air velocity movement, and air composition should be varied within the specified limits. According to standards, the time-weighted average CO_2 in the air composition for premises where people are located should not exceed 1000 ppm (Table 1) [10–13].

Modern methods for calculating gas concentrations in premises and maintaining specified air parameters are mostly based on balance models [10,14,15]. Here, the gas is considered to be evenly distributed on the premises. The CO_2 concentration is measured by sensors installed in arbitrarily selected zones. Based on the data obtained, the mode of air-exchange system operation is controlled, and the regulated air composition is maintained.

Table 1. Indoor air quality classification (EN 13779:2007, GOST 30494-2011) [10–13].

Class	Indoor Air Quality		Acceptable CO_2 Level *, ppm
	Optimal	Permissible	
1	High		400 and less
2	Average		400–600
3		Permissible	600–1000
4		Low	1000 and more

* Allowable CO_2 content in the room is taken over the CO_2 content in the outdoor air outside the room, ppm.

However, recent studies have shown that CO_2 concentrations in the local working area on premises with an operating air-exchange system may not correspond to the average concentrations of pollutants [14,15]. The spatial distribution of carbon dioxide on industrial premises is influenced by many factors: the heat load distribution, the number and location of air inlet and outlet ducts of air-exchange systems, the flow rate and temperature of the supply air, and the location of the CO_2 emission source [16,17]. For example, it was experimentally established that the heat load distribution has a significant effect on the CO_2 distribution in the room [17]. The heated surface intensifies the air movement around it. As a result, the carbon dioxide concentration in this local area decreases. This effect has also been confirmed in numerical simulations [18]. It was found that the heated surface intensified the mixing of air in the local area while reducing the value of the CO_2 concentration by 4.5%. At the same time, the efficiency of air circulation increases by 26.9%.

Heated surfaces in the local working area can significantly affect thermal and concentration fields during the joint operation of open-type gas infrared heaters (CO_2 source) and the air-exchange system [19]. It is also important to mention the established effect of the additional air heating of the local working area [20]. This effect occurs due to the influx of heat released by the GIH case into the air layers around it and their movement into the local working area during air-exchange system operation. It has been experimentally proven that the flow of "fresh" air from the air-exchange system, flowing around the heater case, entrains the gaseous combustion products coming from the GIH burners [20]. As a result, the air-exchange system supplies a mixture of "fresh" air and combustion products to the local working area. This can significantly worsen the air quality in this area. In case of increasing cold airflow from the air-exchange system, the air temperature in the local working area will be significantly reduced. In this regard, it is relevant to analyze the composition of the mixture of gases entering the local working area due to the operation of the gas infrared heater and the air-exchange system.

It Is also reasonable to control t"e airflow in the air-exchange system in order to minimize the gas combustion products influx into the local working area and achieve the maximum possible (within the limits) air temperature in this area. At the same time, the concentration of CO_2 in it will change. However, the analysis and assessment of such changes have not been carried out yet.

The aim of this work was to perform a theoretical analysis of the effect of air-exchange system operation on the thermal conditions and carbon dioxide concentrations in the local working area when using a light-type GIH for the formation of regulated thermal conditions of local working areas.

2. Mathematical Statement of the Problem and Solution Method

Mathematical modeling was carried out within the framework of a two-dimensional approximation for the system shown in Figure 1. A closed rectangular area filled with air was considered, and there was a gas infrared heater (1) and a horizontal panel (simulating equipment) (2) placed in it.

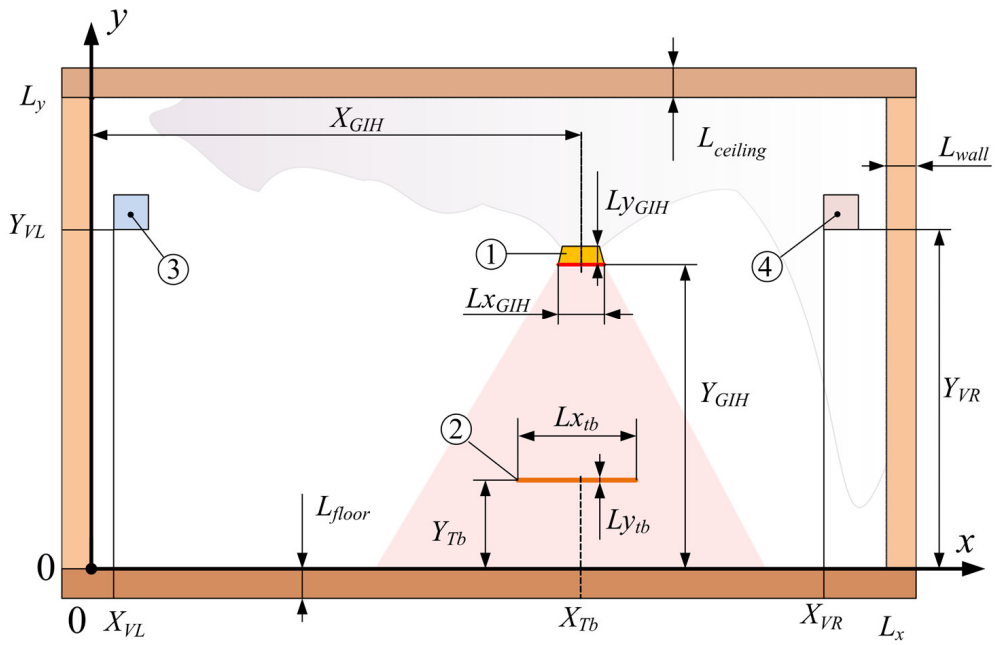

Figure 1. Problem solution area: 1—GIH, 2—panel, 3—air inlet area, 4—air outlet area.

The analysis area also contains the inlet and outlet ducts of the air-exchange system (3 and 4), with the coordinates of the lower left corner $X_{VENT\ left}$, $Y_{VENT\ left}$ and $X_{VENT\ right}$, $Y_{VENT\ right}$. The mathematical model of the considered process involves the creation of the following geometric sets:

1. Total premises volume $A_{\Sigma\ V}$.

$$A_{\Sigma\ V} = \left\{(x,y)\middle| -L_{wall} \le x \le L_x + L_{wall}, -L_{floor} \le y \le L_y + L_{ceiling,}\right\};$$

2. Internal premises volume $A_{\Sigma V\ in}$.

$$A_{\Sigma V\ in} = \left\{(x,y)\middle| 0 \le x \le L_x, 0 \le y \le L_y\right\};$$

3. Exterior surfaces of the premises $A_{\Sigma F\ out}$.

$$A_{\Sigma F\ out} = \left\{(x,y)\middle| \begin{array}{c} x = -L_{wall},\ -L_{floor} \le y \le L_y + L_{ceiling} \\ x = L_x + L_{wall},\ -L_{floor} \le y \le L_y + L_{ceiling} \\ -L_{wall} \le x \le L_x + L_{wall},\ y = -L_{floor} \\ -L_{wall} \le x \le L_x + L_{wall},\ y = L_y + L_{ceiling} \end{array}\right\};$$

4. Interior surfaces of the premises $A_{\Sigma F\ in}$.

$$A_{\Sigma F\ in} = \left\{(x,y)\middle| \begin{array}{c} x = 0,\ 0 \le y \le L_y \\ x = L_x,\ 0 \le y \le L_y \\ 0 \le x \le L_x,\ y = 0 \\ 0 \le x \le L_x,\ y = L_y \end{array}\right\};$$

5. Volume of GIH $A_{\mathrm{GIH}\ V}$.

$$A_{\mathrm{GIH}\ V} = \left\{(x,y)\middle| X_{GIH} - \frac{Lx_{GIH}}{2} \le x \le X_{GIH} + \frac{Lx_{GIH}}{2}, Y_{GIH} \le y \le Y_{GIH} + Ly_{GIH}\right\};$$

6. Total GIH surface $A_{\text{GIH } F}$.

$$A_{\text{GIH } F} = \left\{ (x,y) \left| \begin{array}{c} x = X_{GIH} - \frac{Lx_{GIH}}{2}, \quad Y_{GIH} \le y \le Y_{GIH} + Ly_{GIH} \\ x = X_{GIH} + \frac{Lx_{GIH}}{2}, \quad Y_{GIH} \le y \le Y_{GIH} + Ly_{GIH} \\ X_{GIH} - \frac{Lx_{GIH}}{2} \le x \le X_{GIH} + \frac{Lx_{GIH}}{2}, \quad y = Y_{GIH} + Ly_{GIH} \\ X_{GIH} - \frac{Lx_{GIH}}{2} \le x \le X_{GIH} + \frac{Lx_{GIH}}{2}, \quad y = Y_{GIH} \end{array} \right. \right\};$$

7. Volume of the horizontal panel (table) $A_{\text{Tb } V}$.

$$A_{\text{Tb } V} = \left\{ (x,y) \left| X_{Tb} - \frac{Lx_{Tb}}{2} \le x \le X_{Tb} + \frac{Lx_{Tb}}{2}, Y_{Tb} - Ly_{Tb} \le y \le Y_{Tb} \right. \right\};$$

8. Total surface of the horizontal panel (table) $A_{\text{Tb } F}$.

$$A_{\text{Tb } F} = \left\{ (x,y) \left| \begin{array}{c} x = X_{Tb} - \frac{Lx_{Tb}}{2}, \quad Y_{Tb} - \frac{Ly_{Tb}}{2} \le y \le Y_{Tb} \\ x = X_{Tb} + \frac{Lx_{Tb}}{2}, \quad Y_{Tb} - \frac{Ly_{Tb}}{2} \le y \le Y_{Tb} \\ X_{Tb} - \frac{Lx_{Tb}}{2} \le x \le X_{Tb} + \frac{Lx_{Tb}}{2}, \quad y = Y_{Tb} - Ly_{Tb} \\ X_{Tb} - \frac{Lx_{Tb}}{2} \le x \le X_{Tb} + \frac{Lx_{Tb}}{2}, \quad y = Y_{Tb} \end{array} \right. \right\};$$

9. Volume of the air ducts $A_{\text{VENT } V}$.

$$A_{\text{VENT } V} = \left\{ (x,y) \left| \begin{array}{c} X_{VENTleft} \le x \le X_{VENTleft} + \frac{Lx_{VENT}}{2}, Y_{VENTleft} \le y \le Y_{VENTleft} + Ly_{VENT} \\ X_{VENTright} \le x \le X_{VENTright} + \frac{Lx_{VENT}}{2}, Y_{VENTright} \le y \le Y_{VENTright} + Ly_{VENT} \end{array} \right. \right\};$$

10. Exterior surface of air ducts $A_{\text{VENT } F}$.

$$A_{\text{VENT } F} = \left\{ (x,y) \left| \begin{array}{c} X_{VENTleft} \le x \le X_{VENTleft} + Lx_{VENT}, \ y = Y_{VENTleft} \\ X_{VENTleft} \le x \le X_{VENTleft} + Lx_{VENT}, \ y = Y_{VENTleft} + Ly_{VENT} \\ x = X_{VENTleft}, Y_{VENTleft} \le y \le Y_{VVENTleft} + Ly_{VENT} \\ x = X_{VENTleft} + Lx_{VENT}, Y_{VENTleft} \le y \le Y_{VVENTleft} + Ly_{VENT} \\ X_{VENTright} \le x \le X_{VENTright} + Lx_{VENT}, \ y = Y_{VENTright} \\ X_{VENTright} \le x \le X_{VENTright} + Lx_{VENT}, \ y = Y_{VENTright} + Ly_{VENT} \\ x = X_{VENTright}, Y_{VENTrigh} \le y \le Y_{VENTrigh} + Ly_{VENT} \\ x = X_{VENTrigh} + Lx_{VENT}, Y_{VENTrigh} \le y \le Y_{VENTrigh} + Ly_{VENT} \end{array} \right. \right\}.$$

Inlet and outlet duct areas $A_{\text{VENT } F\ in}$ and $A_{\text{VENT } F\ out}$.

The convective–conductive heat transfer within the assumed physical model was described by the energy equation [21]:

$$\rho c_P \frac{\partial T}{\partial \tau} + \rho c_P \left(\vec{u} \cdot \nabla \right) T = \nabla \cdot (\lambda \cdot \nabla T), \tag{1}$$

$$(x,y) \in A_{\Sigma\ V} \backslash A_{\text{GIH } V} \backslash A_{\text{VENT } V}$$

where $\tau, \rho, T, c_P, \lambda$—time, density, temperature, specific isobaric heat and thermal conductivity, respectively.

The velocity vector field $\vec{u}$ was determined from the solution of the system of equations of motion and the continuity of an incompressible gas in the Boussinesq approximation [22]:

$$\rho \frac{\partial \vec{u}}{\partial \tau} + \rho \left(\vec{u} \cdot \nabla \right) \vec{u} = \nabla \cdot \left[-p \vec{I} + \vec{K} \right] + (\rho - \rho_0) \vec{g}, \tag{2}$$

$$\rho \frac{\partial \vec{u}}{\partial \tau} + \nabla \cdot \left(\rho \vec{u} \right) = 0, \tag{3}$$

$$(x,y) \in A_{\Sigma\ V\ in} \backslash A_{\text{Tb } V} \backslash A_{\text{GIH } V} \backslash A_{\text{VENT } V}.$$

where p, $\vec{I}$—pressure and unit tensor symbol; ρ_0, $\vec{g}$—initial density and gravitational acceleration;

$\vec{K} = (\mu + \mu_T)\left[\nabla\cdot\vec{u} + \left(\nabla\cdot\vec{u}\right)^T\right] - \frac{2}{3}(\mu + \mu_T)\left(\nabla\cdot\vec{u}\right)\vec{I} - \frac{2}{3}\rho k\vec{I}$—viscous friction stress tensor with allowance for the turbulent component ("T" index), μ—dynamic viscosity coefficient.

The "k-ε" model was used for modeling the turbulent airflow. The turbulence kinetic energy (k) and dissipation rate (ε) are described by the equations [23,24]:

$$\rho\frac{\partial k}{\partial \tau} + \rho\left(\vec{u}\cdot\nabla\right)k = \nabla\cdot\left[\left(\mu + \frac{\mu_T}{\sigma_T}\right)(\nabla\cdot k)\right] + P_k - \rho\varepsilon, \tag{4}$$

$$\rho\frac{\partial \varepsilon}{\partial \tau} + \rho\left(\vec{u}\cdot\nabla\right)\varepsilon = \nabla\cdot\left[\left(\mu + \frac{\mu_T}{\sigma_\varepsilon}\right)(\nabla\cdot k)\varepsilon\right] + C_{\varepsilon 1}\frac{\varepsilon}{k}P_{k} - C_{\varepsilon 2}\rho\frac{\varepsilon^2}{k}, \tag{5}$$

$$(x, y) \in A_{\Sigma\ V\ in}\backslash A_{\mathrm{Tb}\ V}\backslash A_{\mathrm{GIH}\ V}\backslash A_{\mathrm{VENT}\ V}.$$

Solutions for Equations (4) and (5) were used to calculate $\mu_T = \rho C_\mu \frac{k^2}{\varepsilon}$. In Equations (4) and (5), the operator had the form $P_k = \mu_T\left[\nabla\cdot\vec{u} : \left(\nabla\cdot\vec{u} + \left(\nabla\cdot\vec{u}\right)^T\right) - \frac{2}{3}\left(\nabla\cdot\vec{u}\right)^2\right] - \frac{2}{3}\rho k\nabla\cdot\vec{u}$. The values of the constants were taken according to the general theory [23,24]:

$$C_{\varepsilon 1} = 1.44, C_{\varepsilon 2} = 1.92, C_\mu = 0.09, \sigma_k = 1, \sigma_\varepsilon = 1.3$$

The generation of turbulence kinetic energy in the region under consideration is concentrated in the area of significant temperature and velocity gradients. Such gradients are localized in the area of forced air injection by the air-exchange system and a limited volume above the GIH. This mechanism of turbulence generation is sufficiently correctly described by the chosen model. As further calculations showed, the influence of turbulence on the intensity of mass, momentum, and energy transfer is significant in these same areas. Also, it has a slight effect on the temperature and concentration fields in the rest of the room, even with significant variations in the parameters affecting the turbulent motion intensity.

Radiation fluxes were calculated using the zonal model [25,26], with a direct integration of fluxes between all components ("Surface-to-Surface Radiation") of a closed system of surfaces with angular coefficients determined within this system.

The carbon dioxide (CO_2) supply was assumed to be carried out from the upper boundary of the GIH. There was no pollution generation within the volume of the solution region. Temperature gradients in the region of analysis were relatively small. Thermal diffusion as a process of the second order of significance can be neglected. Fick's Law was used as a diffusion model for the binary "air-carbon dioxide" diffusion process. The main equation for mass conservation in a non-conservative form, and additionally used relations can be written as follows [21,27]:

$$\rho\frac{\partial \omega_i}{\partial \tau} + \rho\left(\vec{u}\cdot\nabla\right)\omega_i = -\nabla\cdot j_i, \tag{6}$$

$$(x, y) \in A_{\Sigma\ V\ in}\backslash A_{\mathrm{Tb}\ V}\backslash A_{\mathrm{GIH}\ V}\backslash A_{\mathrm{VENT}\ V}.$$

$$j_i = -\left(\rho D_i^f\nabla\omega_i + \rho D_i^f\omega_i\frac{\nabla M_n}{M_n} - j_{c,i}\right), \tag{7}$$

$$M_n = \left(\sum_i\frac{\omega_i}{M_i}\right)^{-1},\ \omega_i\cdot M_n = \chi_i\cdot M_i, \tag{8}$$

$$j_{c,i} = \rho\omega_i\sum_k\frac{M_i}{M_k}D_i^f\nabla\chi_k. \tag{9}$$

The system of Equations (6)–(9) was based on the mass and molar concentrations (ω_i, χ_i), molar masses (M_n) and binary diffusion coefficients (D_i^f). The dependence of the diffusion coefficient D_i^f on temperature was taken into account in the form:

$$D_i^f = D_{i0}^f \left(\frac{T}{T_0}\right)^{1.70} \quad (10)$$

The values of temperatures T_0, zero values of the air velocity components, and the initial value of the mass fraction of CO_2 over the entire area were taken as the initial conditions:

$$T(0,x,y) = T_0, \vec{u}(0,x,y) = 0, \omega_{CO2}(0,x,y) = \omega_{CO2_0},$$
$$(x,y) \in A_{\Sigma\ V} \backslash A_{\text{GIH } V} \backslash A_{\text{VENT } V}.$$

The temperature of the radiating surface of the GIH was set constant on its lower surface for the entire operation time:

$$T(\tau,x,y) = T_{GIH},\ \tau > 0,\ X_{GIH} - \frac{Lx_{GIH}}{2} \le x \le X_{GIH} + \frac{Lx_{GIH}}{2},\ y = Y_{GIH}.$$

During the limited time of GIH operation (work shift), the enclosing structures, as a rule, do not have time to warm up over the entire thickness. Therefore, the conditions of the adiabaticity at the outer boundaries of the solution area were used as boundary conditions for Equation (1):

$$\overrightarrow{\nabla T}(\tau,x,y) = 0, \tau > 0,\ (x,y) \in A_{\Sigma\ F\ out}.$$

On the side surfaces of the GIH:

$$\overrightarrow{\nabla T}(\tau,x,y) = T_{F\ GIH},\ \tau > 0,$$
$$(x,y) \in \left(x = X_{GIH} - \frac{Lx_{GIH}}{2}, Y_{GIH} \le y \le Y_{GIH} + Ly_{GIH}\right) \cup$$
$$\cup \left(x = X_{GIH} + \frac{Lx_{GIH}}{2}, Y_{GIH} \le y \le Y_{GIH} + Ly_{GIH}\right).$$

Here, $T_{F\ GIH}$ is the temperature of the side surfaces of the GIH. Thermocouple measurements show that the $T_{F\ GIH}$ value does not practically depend on the experimental conditions. By the 20th minute of the GIH operation, it reaches the value $T_{F\ GIH} \cong 47 \pm 4$ °C.

On the upper surface of the GIH:

$$\overrightarrow{\nabla T}(\tau,x,y) = -\frac{q_{F\ GIH}}{\lambda}, \tau > 0,$$
$$(x,y) \in \left(X_{GIH} - \frac{Lx_{GIH}}{2} \le x \le X_{GIH} + \frac{Lx_{GIH}}{2}, y = Y_{GIH} + Ly_{GIH}\right).$$

Here, $q_{F\ GIH}$—density of convective heat flux of combustion products. The q_{F_GIE} value was determined by the rated thermal power ($Q_{V\ GIH}$W), radiant efficiency (η_{Rad}) and the upper surface area of the GIH (F_{Up_GIH}, m^2) in accordance with the relationship: $q_{F\ GIH} = (1 - \eta_{Rad}) Q_{V\_GIH} / F_{Up\_GIH}$.

The density of the heat flux to the surface q_{sol} was the sum of the density of the conductive–convective heat flux to this surface q_{gas} and the density of the radiative thermal q_{rad} from all radiating surfaces:

$$q_{sol} = q_{gas} + q_{rad}, \tau > 0,\ (x,y) \in A_{\Sigma\ F\ in} \cup A_{\text{Tb } F}.$$

The no-slip conditions for the "gas-solid surface" interfaces were taken as the boundary conditions for the system of Equations (2) and (3) [22–24].

$$\vec{u}(\tau, x, y) = 0, \tau > 0,$$

$$(x, y) \in A_{\Sigma\ F\ in} \cup A_{\mathrm{Tb}\ F} \cup A_{\mathrm{GIH}\ F} \cup A_{\mathrm{VENT}\ F} \backslash A_{\mathrm{VENT}\ F\ out} \backslash A_{\mathrm{VENT}\ F\ in}.$$

Since the viscous effects prevail over turbulent ones near solid surfaces, the method of near-wall functions was used [22–24].

For the air inlet area $(x, y) \in A_{\mathrm{VENT}\ F\ out}$, the air velocity normal to the surface was set, which can be determined by the mass flow rate, the duct area and the inflow air temperature. For the air outlet area $(x, y) \in A_{\mathrm{VENT}\ F\ out}$, the pressure value was set equal to the atmospheric pressure outside the premises.

It was assumed that air pollution with carbon dioxide occurred due to the combustible gas burning and localizing on the upper GIH surface:

$$j_{CO_2}(\tau, x, y) = j_{GIHCO_2}, \tau > 0,$$

$$(x, y) \in \left(X_{GIH} - \frac{Lx_{GIH}}{2} \le x \le X_{GIH} + \frac{Lx_{GIH}}{2}, y = Y_{GIH} + Ly_{GIH} \right).$$

Based on the heat release rate from the chemical reaction $Q_{V\ GIH}$ and the net calorific value of the fuel Q_{fuel} (J/m^3), the volumetric flow rate of combustible gas for the initial temperature T_{beg} was determined as $V'_{fuel} = \left(Q_{V\ GIH}/Q_{fuel}\right)\left(T_{beg}/273\right)$. The standard fuel formula $C_{\gamma C}H_{\gamma H}$ was used to calculate its molar mass $M_{fuel} = \gamma C{\cdot}12 + \gamma H{\cdot}1$ and mass fraction of carbon $g_{C\ fuel} = \gamma C{\cdot}12/M_{fuel}$. The density of the pollution mass flow was calculated using the formula:

$$j_{GIH\ CO_2} = V'_{fuel} \cdot \frac{p_{beg} \cdot M_{fuel}}{8314 \cdot T_{beg}} \cdot g_{C\ fuel} \cdot \left(\frac{44}{12}\right) / F_{Up\_GIH}. \quad (11)$$

It was assumed that the air coming from the air-exchange system into the premises contains CO_2 in an amount equal to the initial value ω_{CO20}.

The no-flow condition was set for all other solid surfaces:

$$\vec{n} \cdot j_{CO_2}(\tau, x, y) = 0, \tau > 0,$$

$$(x, y) \in A_{\Sigma\ F\ in} \cup A_{\mathrm{Tb}\ F} \cup A_{\mathrm{GIH}\ F} \cup A_{\mathrm{VENT}\ F} \backslash A_{\mathrm{VENT}\ F\ out} \backslash A_{\mathrm{VENT}\ F\ in},$$

$$(x, y) \notin \left(X_{GIH} - \frac{Lx_{GIH}}{2} \le x \le X_{GIH} + \frac{Lx_{GIH}}{2}, y = Y_{GIH} + Ly_{GIH} \right),$$

where $\vec{n}$—unit normal vector to the surface.

The finite element method was chosen for solving the system of Equations (1)–(10) with the corresponding initial and boundary conditions. The COMSOL Multiphysics software environment with modules «The Heat Transfer in Fluids», «The Turbulent Flow» , «Transport of Concentrated Species» and «Surface-to-Surface Radiation» was used.

For a comparative analysis of changes in the average pollution of a room in mass (g_{CO_2}) and volume (r_{CO_2}) fractions, it was assumed that:

1. Mass flows G_{vent} of the air-exchange system (inlet and outlet) were the same;
2. The air mass on the premises m_{room} was constant;
3. The mass carbon dioxide influx on the premises due to combustion did not change the air mass on the premises. It was considered constant and determined by the following: $G_{GIH\ CO_2} = j_{GIH\ CO_2} \cdot F_{Up\_GIH}$.

Under these assumptions, the change in the CO_2 mass on the premises can be described by the following relationship:

$$m_{room}\frac{dg_{CO_2}}{d\tau} = -G_{vent}\left(g_{CO_2} - g_{0CO_2}\right) + G_{GIH\ CO_2} \tag{12}$$

Solutions were obtained by the following transformations:

$$\frac{dg_{CO_2}}{d\tau} = -\frac{G_{vent}}{m_{room}}\left[\left(g_{CO_2} - g_{0CO_2}\right) - \frac{G_{GIH\ CO_2}}{G_{vent}}\right],$$

$$\theta = \left(g_{CO_2} - g_{0CO_2}\right) - \frac{G_{GIH\ CO_2}}{G_{vent}},$$

$$\frac{dg_{CO_2}}{\theta} = -\frac{G_{vent}}{m_{room}}d\tau \Longrightarrow \theta = \theta_0 e^{-\frac{G_{vent}}{m_{room}}\tau},\ \theta_0 = -\frac{G_{GIH\ CO_2}}{G_{vent}}.$$

The $\frac{G_{vent}}{m_{room}}$ value has a clear physical meaning: $Kr = \frac{G_{vent}}{m_{room}} = \frac{\text{Air exchange rate}}{3600}$.
The solution for g_{CO_2} can be written as:

$$g_{CO_2} = g_{0\ CO_2} + \frac{G_{GIH\ CO_2}}{G_{vent}} \cdot \left(1 - e^{-Kr \cdot \tau}\right). \tag{13}$$

A steady-state value of $g_{CO_2\ max}$ is reached at $\tau \longrightarrow \infty$:

$$g_{CO_2\ max} = g_{0\ CO_2} + \frac{G_{GIH\ CO_2}}{G_{vent}}.$$

To determine r_{CO_2}, the following relationship was used:

$$r_{CO_2} = \frac{g_{CO_2}}{44} \cdot \frac{1}{\frac{g_{CO_2}}{44} + \frac{\left(1 - g_{CO_2}\right)}{29}}. \tag{14}$$

The verification of the mathematical model of heat and mass transfer processes in a room with a gas infrared heater (GIH) was conducted using previously obtained experimental data. The experiments examined the thermal state and distribution of combustion products of natural gas (propane) used in a gas infrared heater. The temperatures and concentrations of CO_2, as well as the flow structure in local working areas of a large production facility, were observed.

Experimental studies were carried out in a room with overall dimensions of $5 \times 4.4 \times 11$ m (Figure 2) with an installed light-type GIH-5 of 5 kW nominal thermal power (manufactured by the Sibshvank company, radiant efficiency η_{Rad} = 0.57). An experimental frame made of aluminum pipes with a diameter of 0.015 m with a plastic outer covering was installed in the room. Such a covering allowed us to place a horizontal wood panel ($1.2 \times 0.6 \times 0.04$ m) at different heights from the floor. The panel served as a model of the equipment. The highly thermally conductive material and small diameter of the tubes made it possible to neglect its effect on the generated thermal conditions in the room. The initial temperature was set equal to 7 °C.

The computer, shut-off, and control equipment, as well as a gas cylinder, were located outside the room to eliminate their influence on the thermal conditions of the temperature recording area. The used supply and exhaust ventilation system had an airflow of 420 m^3/h, an air speed of 2.3 m/s at the outlet of the supply channel, and an air temperature of 7 °C. The air ducts were located at a distance of 4 m from the floor (1 m above the GIH). The supply air temperature was kept constant by the operation of the electric air heater. Twelve chromel-alumel-type thermocouples with protection from re-radiation and an insulating coating of PFA fluoropolymer (junction thickness 0.08 mm) were used for temperature measurements. These thermocouples were placed in the local working area at various

points in the zone of the GIH influence. The absolute error in temperature measurement was ±0.2 °C. Changes in CO_2 concentrations in the room and the local working area were recorded by three infrared (NDIR) CO_2 concentration-measurement sensors with a measurement range from 400 to 5000 ppm and an absolute measurement error of ±50 ppm. All the experiments under fixed conditions were carried out at least three times to ensure the possibility of estimating random errors. The standard deviations and corresponding coefficients of variation were calculated. The values of the latter for all experiments did not exceed 4%.

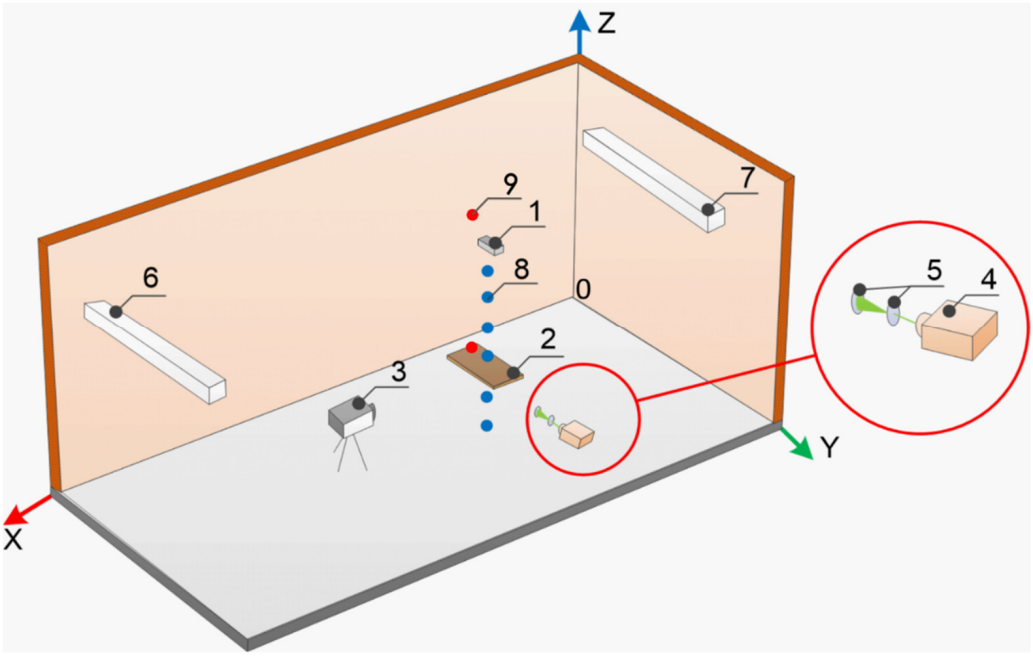

Figure 2. Scheme of the experimental box: 1—GIH; 2—horizontal panel (equipment model); 3—high-speed video camera; 4—laser; 5—system of mirrors for converting the laser beam; 6, 7—openings of the supply and exhaust ventilation system channels; 8, 9—sensors of temperature and CO_2 concentrations, respectively.

Figure 3 presents the main results obtained during the experimental studies.

The experiments have shown that when the surface of the panel is heated, the speed of the air above it increases and the main movement of air masses is directed upward (Figure 3a,b). This is because an increase in the temperature of the panel surface and, accordingly, the air around it (Figure 3c), leads to an increase in thermogravitational forces and air movement velocity and determines its direction (Figure 3a,b). The CO_2 concentration also increases both in the upper part of the room, where the combustion products of natural gas rise, and in the local working area (Figure 3c). This effect is most likely associated with the formation of a large-scale vortex in the room, which is formed during the joint operation of the GIH and the supply and exhaust ventilation system.

Figure 4 shows the distribution of temperatures at the height of the room on the axis of symmetry of the GIH influence zone and CO_2 concentrations in the local working area, established experimentally and numerically.

The deviation of the values of temperatures and CO_2 concentrations obtained during the modeling and experiments (Figure 4) does not exceed 10%. Therefore, it can be concluded that the created mathematical model is applicable for the further research and assessment of the influence of various parameters of the air-exchange system on the structure of air movement and distribution of heat and carbon dioxide in the room.

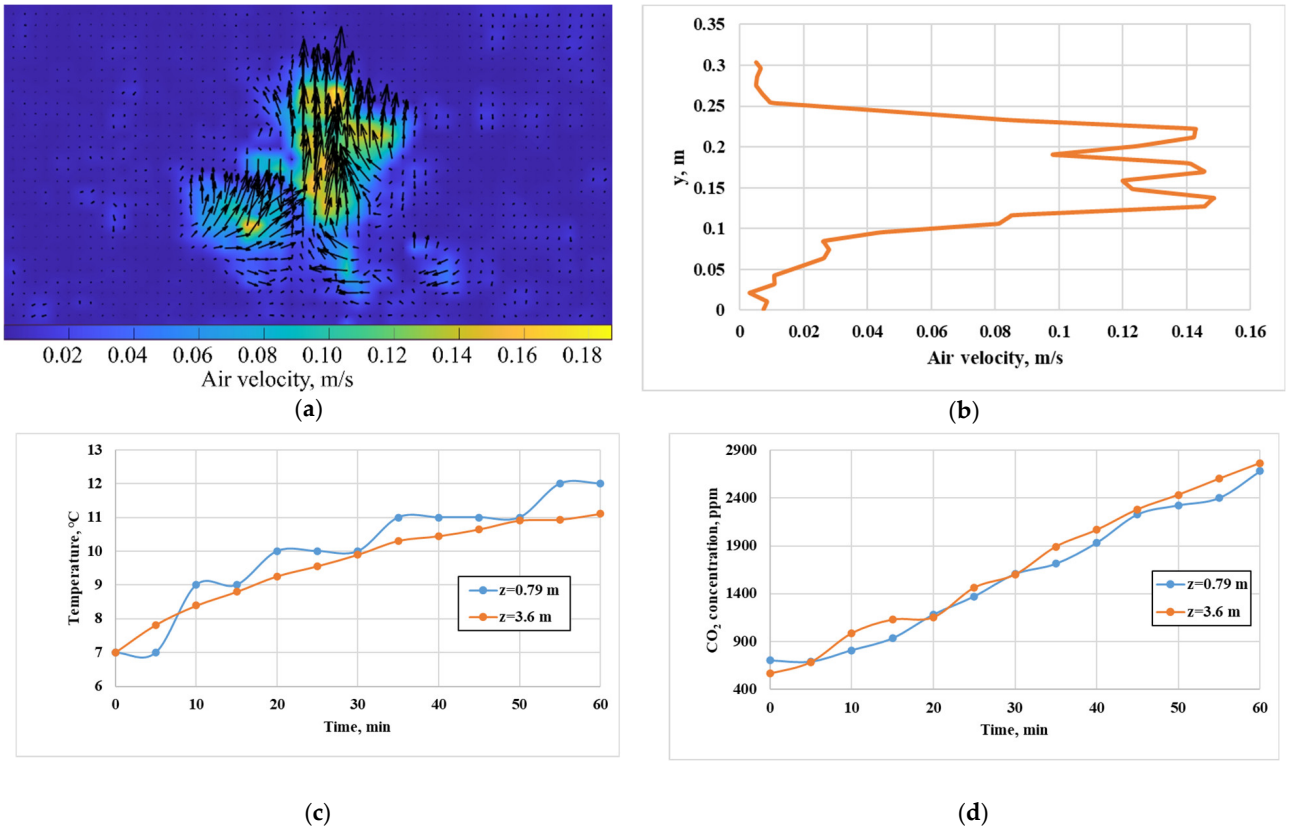

Figure 3. Fields of air movement vectors and speeds (**a**) above the surface of the equipment, speed profile (**b**) at the height from the horizontal surface of the equipment in the central section, as well as changes in air temperature (**c**) and CO_2 concentration (**d**) in time at points z = 0.79 m (local working area) and 3.6 m (upper area in the room at a distance of 0.8 m from the ceiling), y = 6.71 m; x = 3.5 m after 60 min of GIH operation.

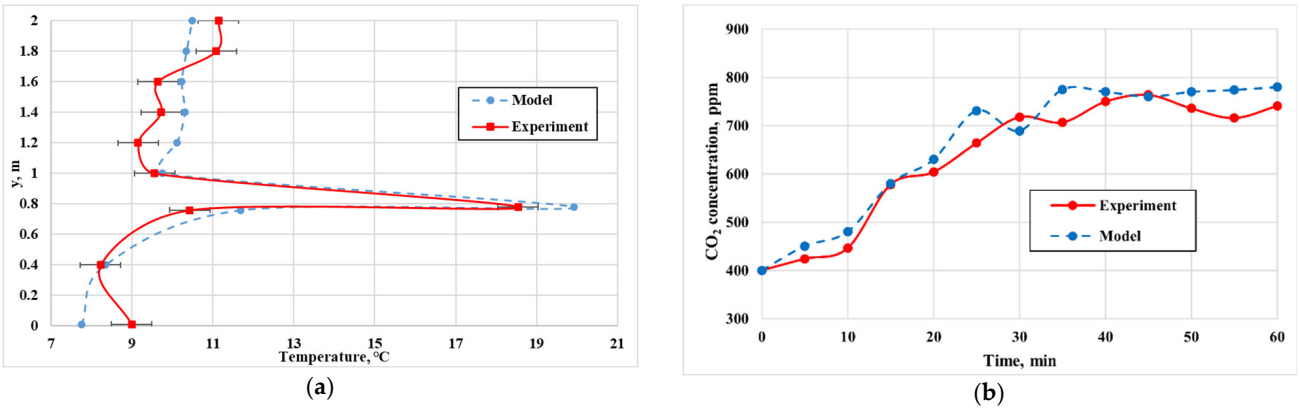

Figure 4. Distributions of experimental and theoretical values of air temperatures along the Y coordinate on the axis of symmetry GIH influence zone (**a**) and CO_2 concentrations in the local working area (z = 0.79 m, y = 6.71 m; x = 3.5 m) after 60 min of GIH operation (**b**).

3. Results

A premises with dimensions of 5 × 4.4 × 11 m was selected for modelling. This premises corresponded to the real one, where experimental studies had been previously carried out [28]. Within the framework of the two-dimensional approximation, a rectangular area with dimensions $L_x = 5 \times L_y = 4.4$ m, bounded by the floor, walls, and ceiling (enclosing structures, Table 2) was considered. The wall thickness was $L_{wall} = 0.1$ m. Two horizon-

tal structural elements (Figure 1) corresponded to the GIH (dimensions Lx_{GIE} = 0.4 m, Ly_{GIE} = 0.05 m) and the equipment element—a horizontal panel (dimensions Lx_{tb} = 0.6 m, Ly_{tb} = 0.04 m).

Table 2. Thermophysical properties of building envelope materials and panels used in experiments [26,29].

Object	l, m	Material	ρ, kg m^{-3}	c, J kg^{-1} K^{-1}	λ, W K^{-1} m^{-1}	ε
Floor, ceiling and walls	0.1	concrete	2500	840	1.55	0.95
Horizontal panel	0.02	pine	520	2300	0.15	0.4

The gas infrared heater had a power of $Q_{VGIH} = 5$ kW. Propane (C_3H_8) with a calorific value $Q_{fuel} = 93,370$ kJ/m^3 was used as the working gas [26,29]. The CO_2 mass flow in this case was 3.1547×10^{-5} kg/s.

The value of 7 °C was taken as the initial temperature of all analyzed areas. The temperature of the incoming air from the air-exchange system was also 7 °C. The mass flow rate of the inlet part of the air-exchange system vent was varied in a range from 0.02 to 2 kg/s (9.09×10^{-5} to 9.09×10^{-3} kg/(s × m^3)).

The parameters from the COMSOL Multiphysics Materials Library were used as initial values for the air thermal properties. The main thermophysical parameters of the enclosing structures and the horizontal panel are presented in Table 2.

Previous studies showed that within 40–60 min from the start of a complex process of the mutual influence of thermogravitational and forced convection, caused by the GIH and air-exchange system operation, respectively, a stationary hydrodynamic picture of the air masses movement and the corresponding temperature field can be mainly established [1,28]. As the value of the average temperature over the volume of the premises is reached, the sufficiently intense changes in velocity and temperature ends. The average temperature over the volume corresponds to approximately 87% of the maximum value of the average temperature over the volume [28], which characterizes the stationary distribution of temperature fields. In this case, the representative fields of velocities and temperatures topologically and practically cease to change with time. Only the magnitudes of the maximum and minimum values change insignificantly. Therefore, the results of calculating the characteristics of processes by the time of 60 min are presented and analyzed below.

The fields of velocities, temperatures and mass concentrations of CO_2, as well as their distributions at the height of two vertical sections with coordinates x = 0.8 m (20 cm to the left of the panel) and x = 2.4 m (to the right of the panel 20 cm) in the possible working areas, are presented in Figures 5–14. In Figure 5, Figure 7, Figure 9, Figure 11 two white squares are the input and output areas of the air exchange system and the single rectangle is the radiator area (Figure 1). These areas are excluded from the simulation, and accordingly, they are white in the figures (there are no values for them, and in the color palette it is white color).

According to the standards, comfortable conditions are characterized not only by the temperature values but also by minimum temperature differences in height from the floor level to the upper limit of the local working area [10–13,30].

The flow pattern formed at the flow rate of blown air of 0.02 kg/s (9.09×10^{-5} kg/(s × m^3)) (Figure 5) is a consequence of air movement due to the air-exchange system operation and thermogravitational convection.

The results of numerical analysis (Figure 5) show that the cold air from the air inlet duct of the air-exchange system deviates from the horizontal path downwards. When flowing into the GIH, it is divided into two parts. Most of it deflects the upward flow of hot combustion products to the right towards the outlet duct. Some of these products, mixed with air from the air-exchange system and cooled near the right wall, move down. Then, meeting with more heated surfaces of the floor and the horizontal panel surface, they

form an upward flow. The second part of the air from the inlet part of the air-exchange system goes around the GIH from below. In the opposite direction, an upward flow moves from a heated horizontal surface of a panel that simulates the equipment. The interaction of these flows forms three main recirculation zones in the central area along the height of the premises. The currents flow clockwise on the left and right near the walls and counterclockwise in the central part. As a result, carbon dioxide accumulates in the ceiling area (mostly to the right of the GIH), then spreads, and, together with downward flows, falls down. At the same time, the asymmetry of the horizontal panel location and the ascending flows formed from it prevent the left flow with CO_2 from reaching the floor. On the right, the flow of CO_2 reaches the floor and gradually increases the degree of air pollution in the lower right corner of the region. Figure 6 shows the temperature and CO_2 concentration profiles in local work areas to the left and right of the equipment model.

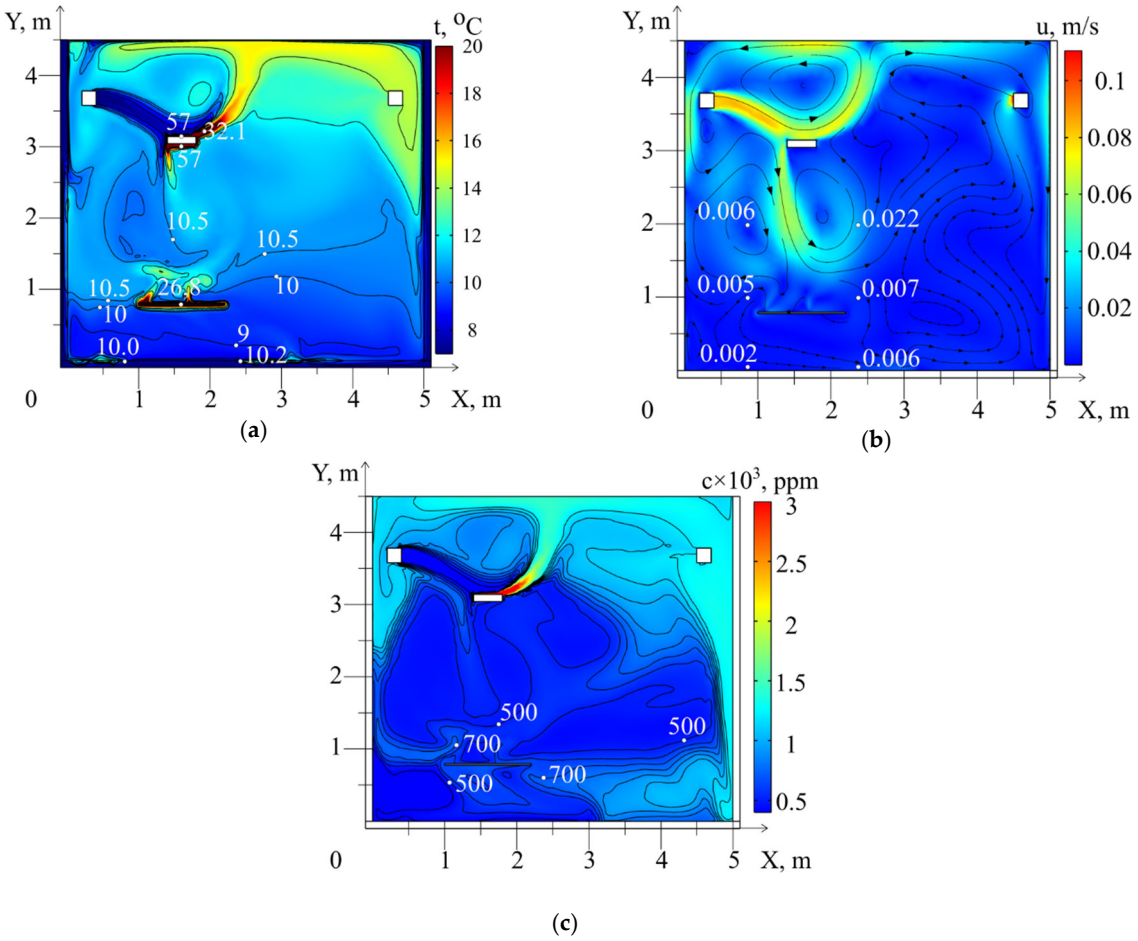

Figure 5. Fields of temperatures (**a**), air velocities (**b**) and CO_2 concentrations (**c**), formed by the 60th minute of the GIH operation at an airflow rate of 0.02 kg/s (9.09×10^{-5} kg/(s × m^3)).

An increase in airflow up to 0.04 kg/s (18.2×10^{-5} kg/(s × m^3)) changes the ratio between the effect of forced and thermogravitational convection (Figure 7). In this case, the air moves almost horizontally from the inlet to the outlet duct, and the air ascending from the horizontal panel reaches the air inlet duct of the air-exchange system. Two recirculation zones are formed in the area central to the height of the premises. Their formation is mainly influenced by the descending flows of air cooled by the walls and the ascending warm flow from the horizontal panel. Such a flow distribution increases the temperature and concentration of CO_2 in the central and left areas of the premises. As a result, it affects the distribution of the temperatures and concentrations of CO_2 at the height in the working area to the left and right of the horizontal panel (Figure 8).

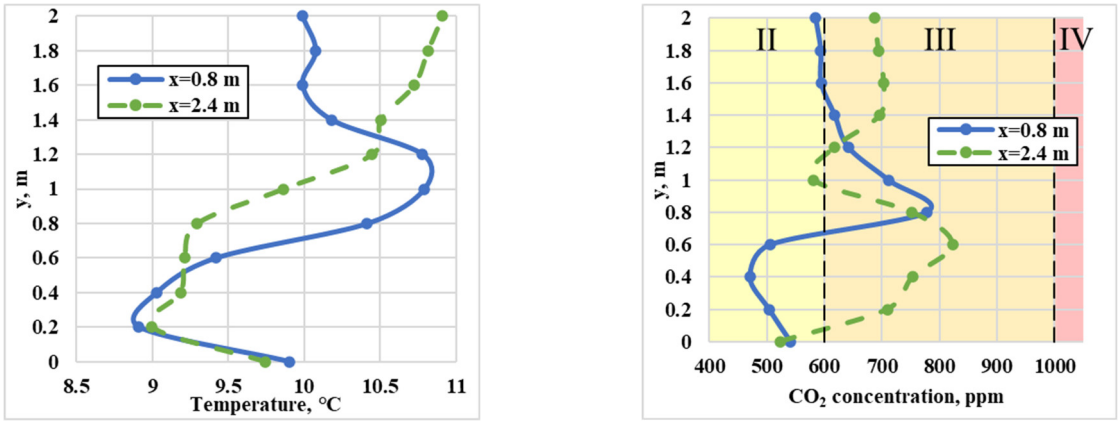

(**a**) (**b**)

Figure 6. Temperature profiles (**a**) and CO_2 concentration (**b**) formed by the 60th minute of the GIH operation at an airflow rate of 0.02 kg/s (9.09×10^{-5} kg/(s × m^3)). II–IV—indoor air quality class (Table 1).

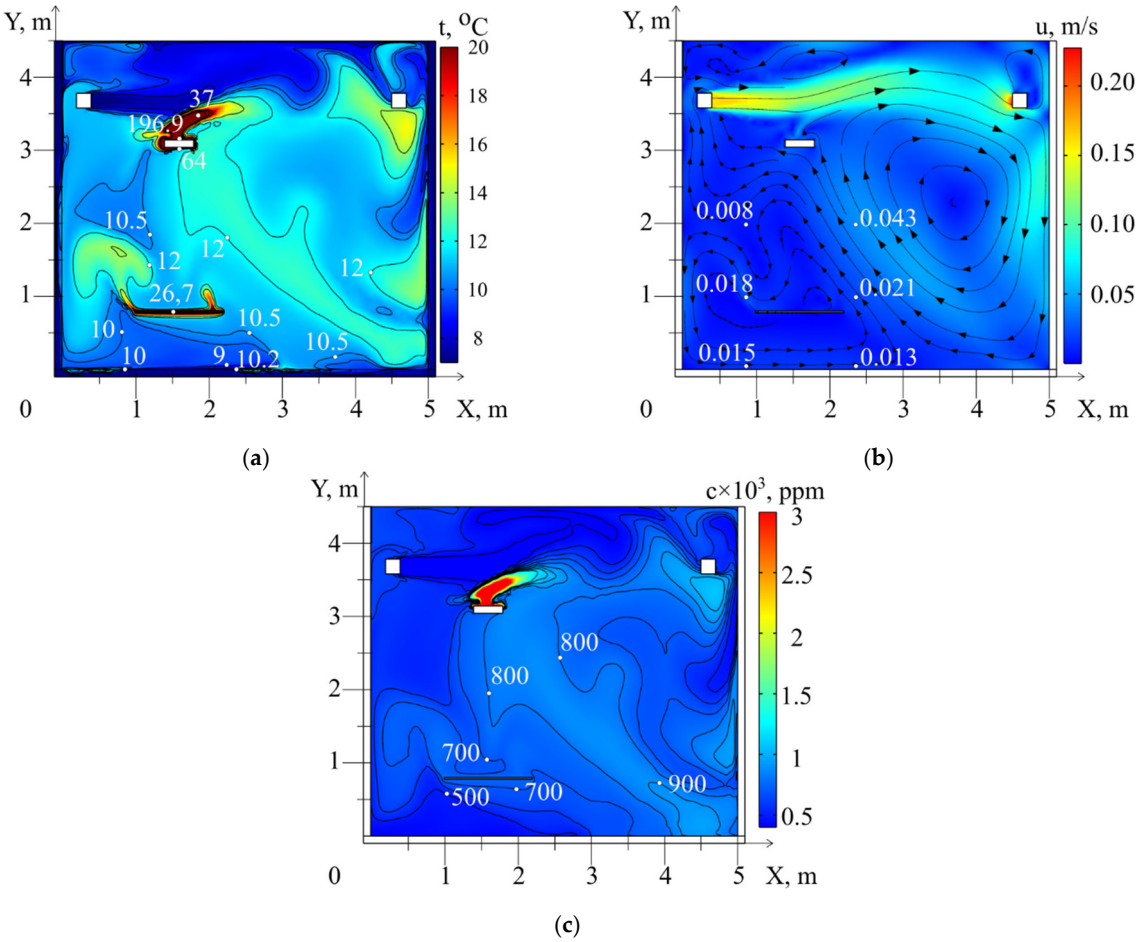

(**a**) (**b**) (**c**)

Figure 7. Fields of temperatures (**a**), air velocities (**b**) and CO_2 concentrations (**c**), formed by the 60th minute of the GIH operation at an airflow rate of 0.04 kg/s (18.2×10^{-5} kg/(s × m^3)).

At the same time, the air temperature in the local area to the right of the table rises to 14 °C (3 degrees (27%), compared with G_{vent} = 0.02 kg/s (9.09×10^{-5} kg/(s × m^3)). The CO_2 concentration also increases up to 870 ppm but does not exceed the acceptable value.

A further increase in the flow rate of the injected air up to 0.07 kg/s (31.8×10^{-5} kg/(s × m^3)) contributes to a significant increase in the recirculation flow intensity (Figure 9). This flow accumulates warm air in the central area of the premises and leads to an increase in temperature and carbon dioxide concentration in this part of the premises.

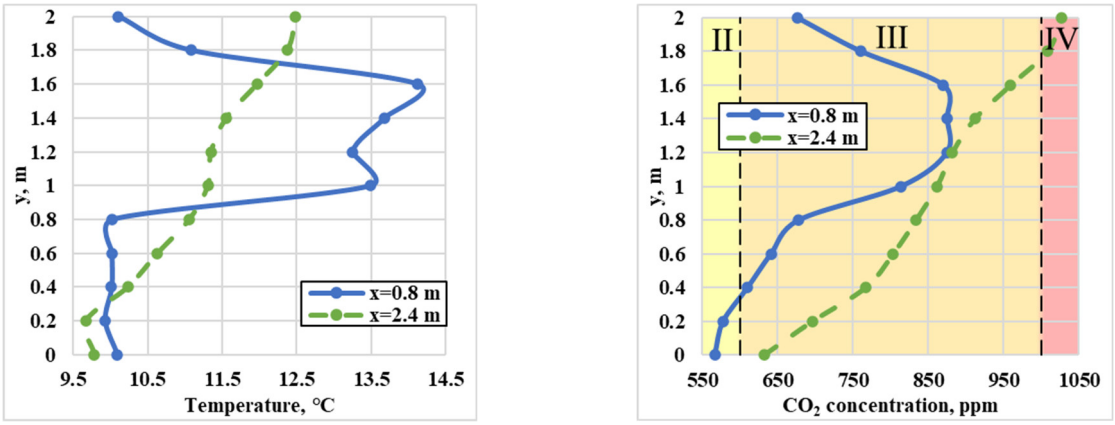

(**a**) (**b**)

Figure 8. Temperature profiles (**a**) and CO_2 concentration (**b**) formed by the 60th minute of the GIH operation at an airflow rate of 0.04 kg/s (13.6×10^{-5} kg/(s × m^3)). II–IV—indoor air quality class (Table 1).

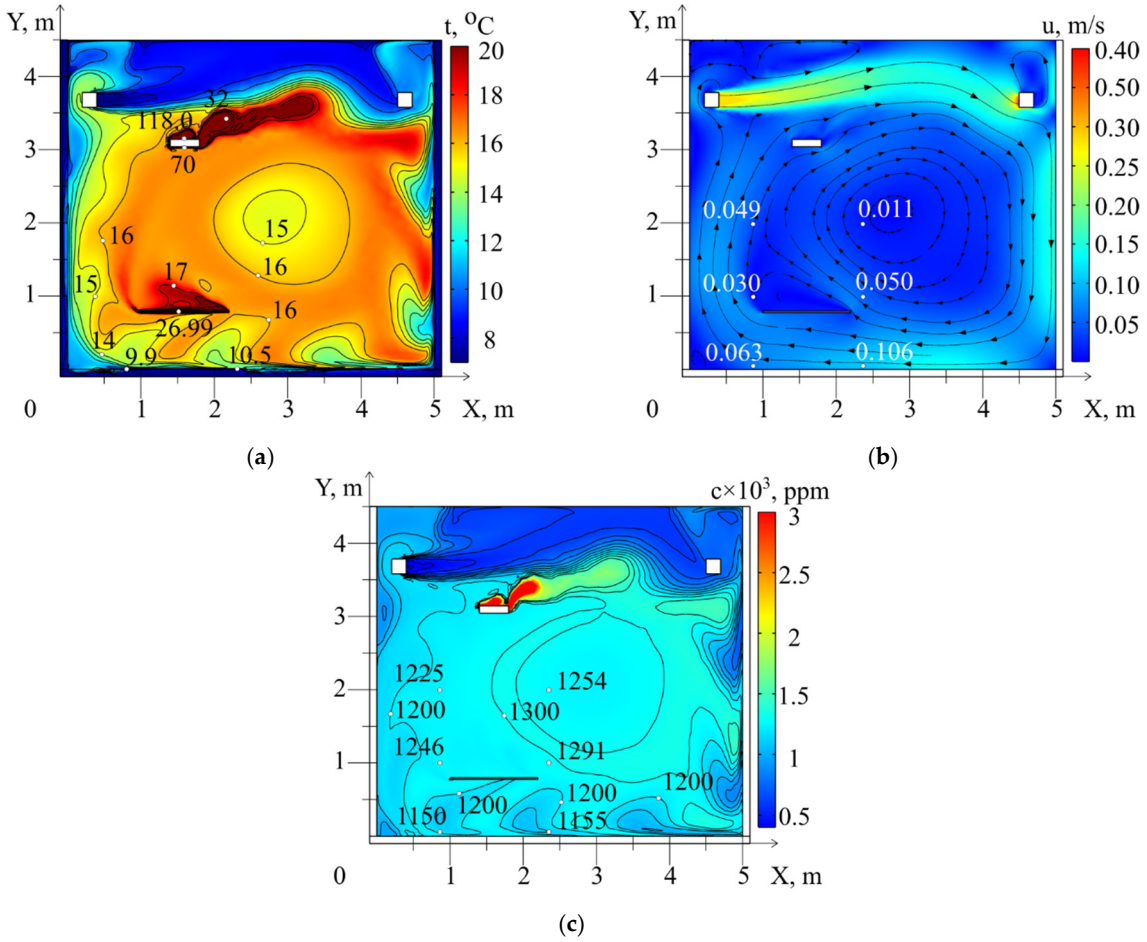

(**a**) (**b**) (**c**)

Figure 9. Fields of temperatures (**a**), air velocities (**b**) and CO_2 concentrations (**c**), formed by the 60th minute of the GIH operation at an airflow rate of 0.07 kg/s (31.8×10^{-5} kg/(s × m^3)).

An analysis of the obtained results shows that a significant increase in the arrival of a cold flow forms a pronounced recirculation flow along the enclosed structures, which forms relatively narrow near-wall areas near the latter. Warm air from the GIH and the horizontal panel accumulates in the peripheral part of the recirculation flow and gradually fills its central part with an increase in the discharge flow rate. It should be noted that, despite a sufficiently significant increase in air temperatures, air pollution in the working areas remains below the permissible values.

The results of the numerical simulation also show that the distribution of air heated from the GIH surface to the upper enclosing structure is hindered by a more intense flow of cold air from the air-exchange system, which moves almost horizontally to the middle of the study area.

In the section X > 3 m, the velocity of the airflow blown into the premises slows down (Figure 9b) to 0.1 m/s. The colder air from the inlet of the air-exchange system pushes down the heated layers of air (Figure 9a). As a result, warm air moves towards the right building envelope below the outlet of the air-exchange system.

As a result, with an increase in airflow up to 0.07 kg/s (31.8×10^{-5} kg/(s × m^3)), the air temperature in the central part of the premises rises, although the injected air has a significantly lower temperature than that in the working areas (Figure 10). But as a consequence of such a circulation flow, CO_2 also enters the local working area along with the air heated from the GIH. The gas concentration increases to the right of the panel from 850 ppm to 1200 ppm (higher than the allowable one) (Figures 8b and 10b).

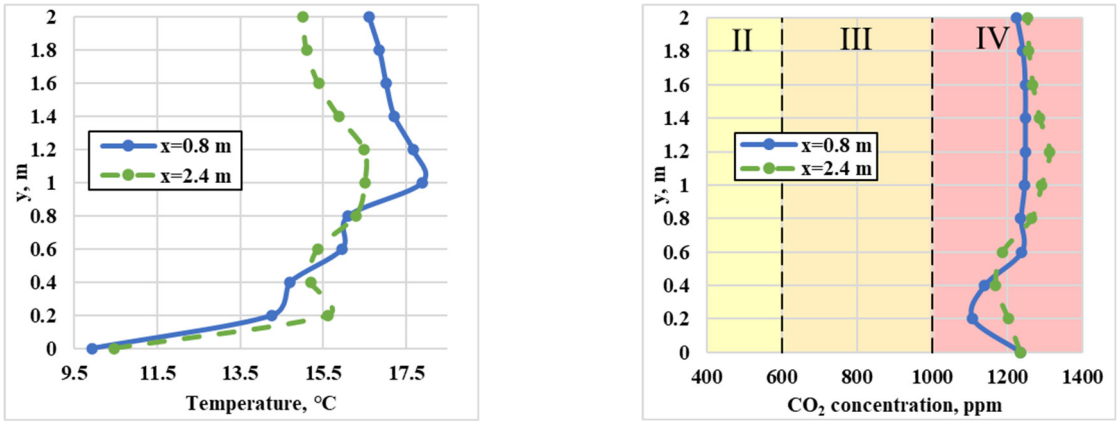

(**a**) (**b**)

Figure 10. Temperature profiles (**a**) and CO_2 concentration (**b**) formed by the 60th minute of the GIH operation at an airflow rate of 0.07 kg/s ($31.8 \cdot 10^{-5}$ kg/(s·m^3)). II–IV—indoor air quality class (Table 1).

The subsequent increase in the air circulation ratio (40.9×10^{-5} kg/(s × m^3)) leads to the division of the solution area into two main circulation zones (Figure 11), located almost horizontally relative to each other.

The first zone is formed above the GIH. The blown air from the air-exchange system flows at a sufficiently high speed to the outlet area, practically without interacting with the air in the central part of the room. The second circulation zone is located below the inlet and outlet ventilation holes (Figure 11b). The air heated from the GIH case circulates in the lower part of the premises. The distribution of temperatures (Figure 12a) and concentrations (Figure 12b) in the local working area increases.

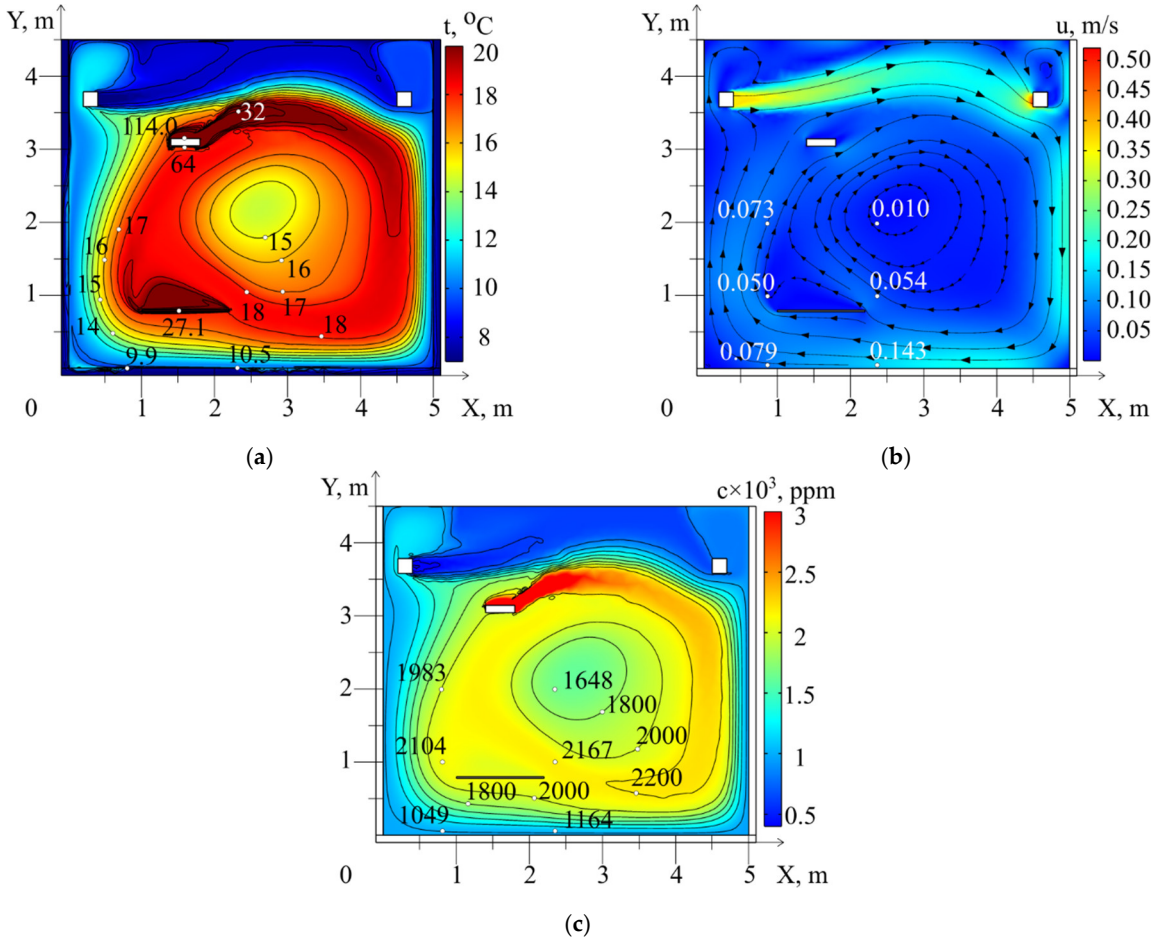

Figure 11. Fields of temperatures (**a**), air velocities (**b**) and CO_2 concentration (**c**), formed by the 60th minute of the GIH operation at an airflow rate of 0.09 kg/s (40.9 × 10^{-5} kg/(s × m^3)).

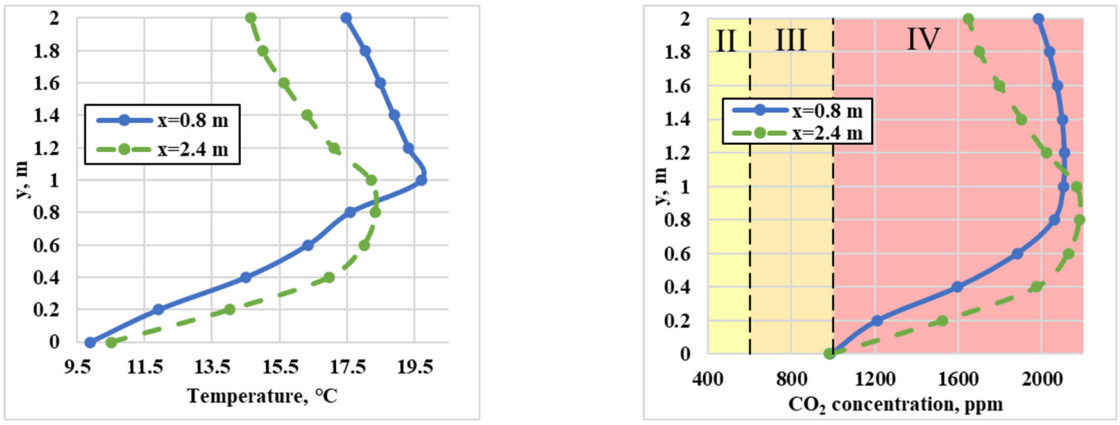

Figure 12. Temperature profiles (**a**) and CO_2 concentration (**b**) formed by the 60th minute of the GIH operation at an airflow rate of 0.09 kg/s (40.9 × 10^{-5} kg/(s × m^3)). II–IV—indoor air quality class (Table 1).

Figure 13 shows changes in the CO_2 average concentration in the premises volume, depending on the flow rate of the air-exchange system. The results were obtained on the basis of solving balance Equations (13) and (14) (used in the calculation methods of ventilation systems [5–8]).

An analysis of the results showed that for fairly typical premises with a working GIH and an air-exchange system, the standard concentrations for CO_2 content in the air (no more than 1000 ppm) are achieved at an airflow rate in the air-exchange system of at least 0.31 kg/s (Figure 13a). However, the excess of the limiting concentration of CO_2 in the premises volume is reached after 20–30 min at lower airflow rates.

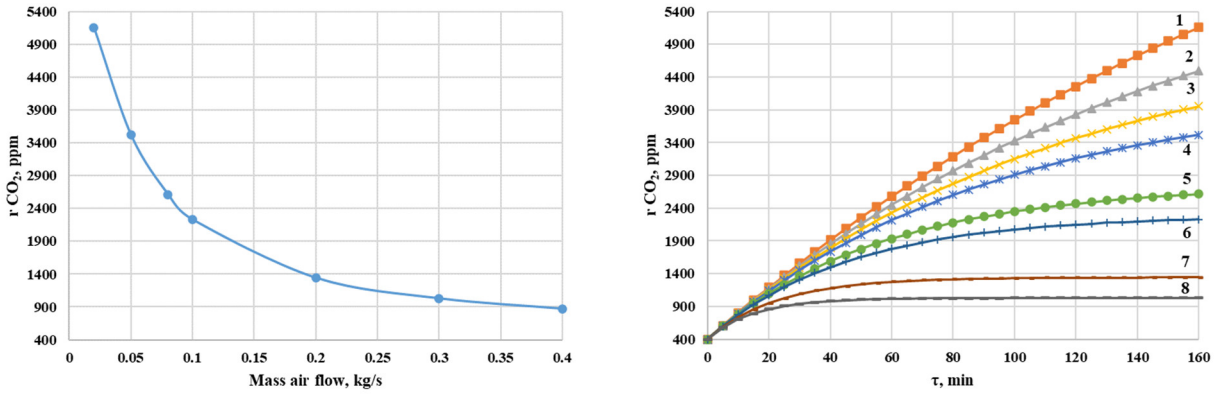

(**a**) (**b**)

Figure 13. Dependence of the average CO_2 concentration over the volume of the premises on the airflow in the air-exchange system (**a**) at τ = 160 min and its change in time (**b**) at airflow rates in the air-exchange system: 1—0.02 kg/s, 2—0.03 kg/s c, 3—0.04 kg/s, 4—0.05 kg/s, 5—0.08 kg/s, 6—0.1 kg/s, 7—0.2 kg/s, 8—0.3 kg/s.

At the same time, the simulation results (Figures 5–11) show that intensive air mixing in the room does not occur during the joint operation of the gas infrared heater and the air-exchange system (the main assumption in calculations using balance models). Zones with significantly different CO_2 concentrations are formed. Heated and carbon dioxide-polluted air is mainly located in the upper part of the premises. The CO_2 concentration values remain within acceptable limits in the local working areas. It can be concluded that when forming the thermal conditions in the local working area using a GIH, it is possible to maintain the standard conditions for CO_2 concentration with a lower consumption of air from the air-exchange system. This is especially true if the formation of a thermal area is required for a short time (from 30 min to 1.5 h). For example, according to the results of numerical simulation (Figure 14), with an airflow rate of 0.04 kg/s, a worker can stay in the local working area for quite a long time (about 120 min). However, according to balance models calculations, this time is 20 min and below (six times less) (Figure 13b).

A significant increase in airflow in the air-exchange system leads to an intensification of the air mass movement (mixing). In this case, both the temperature and the CO_2 concentration in the local working areas increase. For the range of airflow rates from 0.05 to 0.6 kg/s, CO_2 concentrations are above the critical level (from 1000 to 2000 ppm) (Figure 12). With a further increase in airflow in the air-exchange system to 0.1 kg/s, the temperature and CO_2 concentration in the local working area increase to the maximum (17 °C, 2000 ppm) (Figure 15). In the central part of the premises, an extensive circulation vortex is formed, into which combustion products from the GIH enter, but a further increase in the consumption of the air-exchange system leads to a decrease in both temperature (to 11–13 °C) and CO_2 concentration (tends to the initial—400 ppm) in local working areas (Figure 12b). This circumstance is a consequence of the increasing excess of the mass of incoming air over the flow of hot combustion products coming from the gas infrared heater.

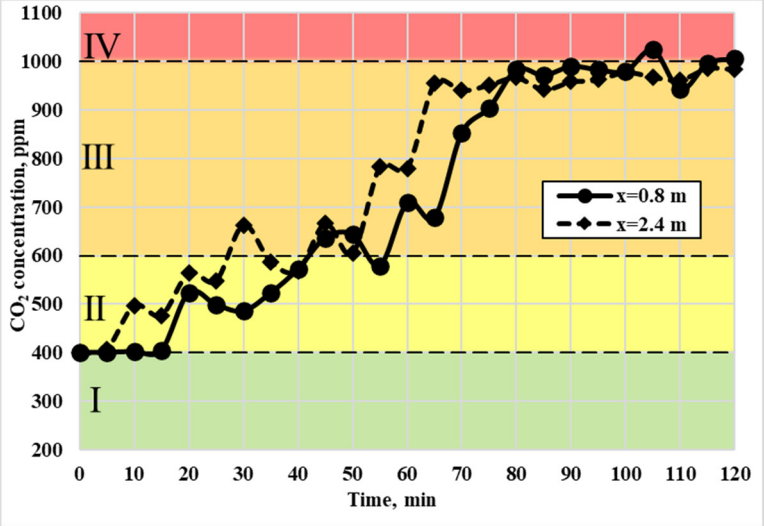

Figure 14. Dependence on time of the average value of CO_2 concentration at heights from 0 to 2 m in the working areas with a flow rate of ventilated air of 0.04 kg/s (18.2×10^{-5} kg/(s × m^3)). I–IV—indoor air quality class (Table 1).

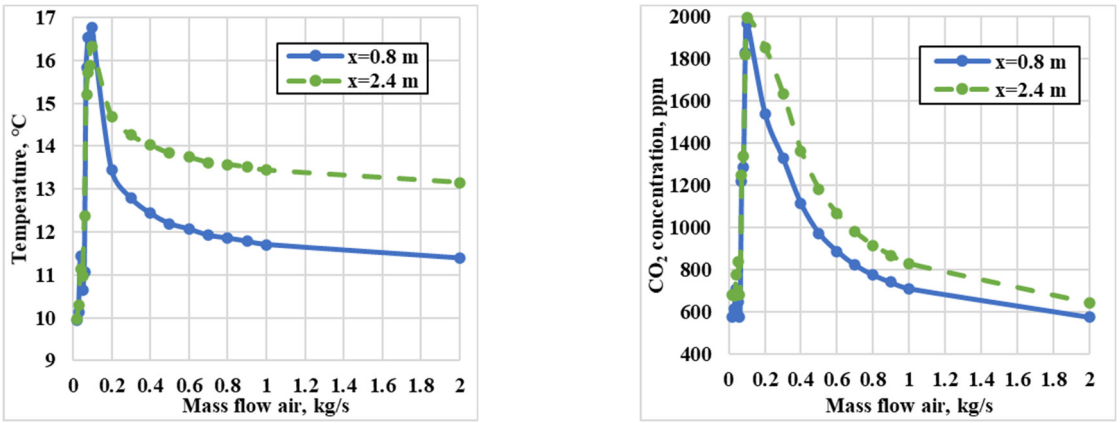

(**a**) (**b**)

Figure 15. Dependence of the height-average air temperature (**a**) and CO_2 concentration (**b**) in local working areas to the left (x = 0.8 m) and to the right (x = 2.4 m) of the table by 20 cm from the airflow after 60 min of GIH operation.

The analysis of the numerical simulation results also showed that the necessary airflow rate from the air-exchange system to create regulated conditions for CO_2 concentration in the air (less than 1000 ppm) lies in the ranges from 0.02 to 0.04 kg/s and from 0.6 kg/s (Figure 15). The calculated air consumption according to the method based on balance models is 0.31 kg/s (outside this range).

4. Conclusions

A theoretical analysis of the effect of air-exchange system operation on the thermal conditions and carbon dioxide concentration of a local working area when using a light-type GIH was carried out. The numerical study of the processes was carried out using the COMSOL Multiphysics environment. Using the k-ε model made it possible to take into account the influence of turbulent flow. Changing the turbulence model from within the simulation environment range and its intensity parameters did not significantly affect the temperature and concentration fields in a larger volume of the room. This is due to the fact that the turbulence generation was localized in extremely limited volumes, positioned in the zone of forced air inflow from the air-exchange system and above the GIH. Such a case

can be well described by the k-ε turbulence model. It was established that two zones with quite significantly different CO_2 concentrations and air temperatures are formed during GIH operation. The airflow in the air-exchange system significantly affects the formation of such zones in the room. At low airflow rates up to 0.04 kg/s (18.2×10^{-5} kg/(s × m^3)), a zone of air heated and highly concentrated by carbon dioxide is formed in the upper part of the room. It was found that with an airflow rate of 0.04 kg/s (13.6×10^{-5} kg/(s × m^3)), it is possible to direct some of the heated air to the local working area, increasing the air temperature by 27% without the CO_2 concentration exceeding the regulated value (less than 1000 ppm).

Author Contributions: Conceptualization, G.V.K.; methodology, V.I.M. and G.V.K.; software, V.I.M. and B.V.B.; validation, B.V.B., V.I.M. and F.Y.S.; formal analysis, V.I.M.; investigation, F.Y.S. and T.A.N.; writing—original draft preparation, F.Y.S.; writing—review and editing, T.A.N.; visualization, F.Y.S. and T.A.N.; supervision, G.V.K.; project administration, G.V.K.; funding acquisition, V.I.M. All authors have read and agreed to the published version of the manuscript.

Funding: This work is supported by the Russian Science Foundation (number grant 20-19-00226).

Data Availability Statement: Data available on request due to restrictions of institution.

Conflicts of Interest: The authors declare no conflicts of interest.

References

1. Kuznetsov, G.V.; Kurilenko, N.I.; Maksimov, V.I.; Nagornova, T.A. Experimental and numerical study of heat transfer in production area heated by gas infrared source. *Int. J. Therm. Sci.* **2020**, *154*, 106396. [CrossRef]
2. Dudkiewicz, E.; Szałański, P. Overview of exhaust gas heat recovery technologies for radiant heating systems in large halls. *Therm. Sci. Engin. Progress.* **2020**, *18*, 100522. [CrossRef]
3. Kavga, A.; Karanastasi, E.; Konstas, I.; Panidis, T. Performance of an Infrared Heating System in a Production Greenhouse. *IFAC Proc.* **2013**, *46*, 235–240. [CrossRef]
4. Dudkiewicz, E.; Fidorów-Kaprawy, N.; Szałański, P. Environmental benefits and energy savings from gas radiant heaters' flue-gas heat recovery. *Sustainability* **2022**, *14*, 8013. [CrossRef]
5. Mikhailova, L.Y.; Kurilenko, N.I.; Germanova, T.V.; Shcherbakova, E.N. Decentralized heat supply systems for industrial buildings using natural gas from the Arctic zone. *IOP Conf. Series. Earth Environ. Sci.* **2022**, *990*, 012066. [CrossRef]
6. Industrial Heating Systems by Schwank. Available online: https://schwank.co.uk/products/industrial-heating-systems/?lang=en (accessed on 15 November 2023).
7. Peng, P.; Zhang, C.; Li, W.; Pomianowski, M.; Gong, G.; Fang, X.; Chun, L.; Guo, R. Investigation on indoor airflow and contaminant dispersion of diffuse ceiling ventilation in heating and cooling modes. *J. Build. Eng.* **2023**, *80*, 107972. [CrossRef]
8. Zhang, C.; Pomianowski, M.; Heiselberg, P.K.; Yu, T. A review of integrated radiant heating/cooling with ventilation systems—Thermal comfort and indoor air quality. *Energ. Build.* **2020**, *223*, 110094. [CrossRef]
9. Maher, D.; Hana, A.; Arjmand, J.T.; Issakhov, A.; Sammouda, H.; Sheremet, M.; Sharma, S. Effect of inlet/outlet on thermal performance of naturally ventilated building. *Int. J. Low Carbon Technol.* **2021**, *16*, 1348–1362. [CrossRef]
10. *GOST 30494-2011*; Residential and Public Buildings. Microclimate Parameters for Indoor Enclosures: Moscow, Russia, 2011.
11. *EN 13779:2007*; Ventilation for Non-Residential Buildings. Performance Requirements for Ventilation and Room-Conditioning Systems: Moscow, Russia, 2007.
12. *ISO 7730*; Moderate Thermal Environment—Determination of the PMV and PPD Indices and Specification of the Conditions for Thermal Comfort. International Organization for Standardization: Geneva, Switzerland, 2005.
13. *EN 16798-1:2019*; Energy Performance of Buildings—Ventilation for Buildings—Part 1: Indoor Environmental Input Parameters for Design and Assessment of Energy Performance of Buildings Addressing Indoor Air Quality, Thermal Environment, Lighting and Acoustics—Module M1-6. CEN-CENELEC Management Centre: Brussels, Belgium, 2019.
14. Majumdar, D.; Chatterjee, S. Modelling accumulation of respiratory-CO_2 in closed rooms leading to decision-making on room occupancy. *MAPAN-J. Metrol. Soc. India* **2020**, *35*, 323–332. [CrossRef]
15. Zhang, D.; Zhang, L. Experimental and simulation research on indoor CO_2 removal efficiency and fresh air energy savings of living walls in office spaces. *Preprints* **2023**. [CrossRef]
16. Bivolarova, M.; Snaselova, T.; Markov, D.; Melikov, A.K. CO_2 based ventilation control—importance of sensor positioning, CO_2 Based Ventilation Control—Importance of Sensor Positioning. In Proceedings of the 15th ROOMVENT Virtual Conference, Torino, Italy, 15–17 February 2021.
17. Snaselova, T.; Bivolarova, M.; Markov, D.; Melikov, A. Exposure to metabolic CO_2 in a room with mixing air distribution. In Proceedings of the 15th ROOMVENT Virtual Conference, Torino, Italy, 15–17 February 2021.
18. Keli, A.; Melikov, A.K.; Bivolarova, M.P.; Mustakallio, P. Impact of room airflow interaction on metabolic CO_2 exposure. *E3S Web Conf.* **2019**, *111*, 02005. [CrossRef]

19. Borisov, B.V.; Vyatkin, A.V.; Kuznetsov, G.V.; Maksimov, V.I.; Nagornova, T.A. Mathematical modeling of heat transfer in a room with a gas infrared emitter, an air exchange system, and a local fence of the working area. *J. Appl. Ind. Math.* **2023**, *17*, 15–24. [CrossRef]
20. Borisov, B.V.; Vyatkin, A.V.; Kuznetsov, G.V.; Maksimov, V.I.; Nagornova, T.A. Numerical Analysis of the Influence of the Air Exchange System Configuration on the Temperature Regime of Local Working Areas in a Room with a Gas Infrared Heater. *Bull. Tomsk Polytech. Univ. Geo Assets Eng.* **2023**, *334*, 7–16. [CrossRef]
21. Bird, B.; Stewart, W.E.; Lightfoot, E.N. *Transport Phenomena*, 2nd ed.; John Wiley & Sons: Hoboken, NJ, USA, 2007.
22. Tritton, D.J. *Physical Fluid Dynamics*, 2nd ed.; Clarendon Press: Oxford, UK, 1988.
23. Wilcox, D.C. *Turbulence Modeling for CFD*, 2nd ed.; DCW Industries: Canada, CA, USA, 1988.
24. Kuzmin, D.; Mierka, O.; Turek, S. On the Implementation of the k-ε Turbulence Model in Incompressible Flow Solvers Based on a Finite Element Discretization. *Int. J. Comput. Sci. Math.* **2007**, *1*, 193–206. Available online: https://www.researchgate.net/publication/228529803 (accessed on 25 December 2023). [CrossRef]
25. Siegel, R.; Howell, J. *Thermal Radiation Heat Transfer*, 4th ed.; Taylor & Francis: New York, NY, USA, 2002.
26. Haynes, W.M. *Handbook of Chemistry and Physics 2015–2016*; CRC/Taylor & Francis: Boca Raton, FL, USA, 2015.
27. Curtiss, C.F.; Bird, R.B. Multicomponent Diffusion. *Ind. Chem. Res.* **1999**, *38*, 2515–2522. [CrossRef]
28. Borisov, B.V.; Vyatkin, A.V.; Kuznetsov, G.V.; Maksimov, V.I.; Nagornova, T.A. Analysis of the Influence of the Gas Infrared Heater and Equipment Element Relative Positions on Industrial Premises Thermal Conditions. *Energies* **2022**, *15*, 8749. [CrossRef]
29. DOE Fundamentals Handbook. *Thermodynamics, Heat Transfer and Fluid Flow (Volume 2 of 3)*; U.S. Department of Energy: Washington, DC, USA, 2016.
30. Karmann, C.; Schiavon, S.; Bauman, F. Thermal comfort in buildings using radiant vs. all-air systems: A critical literature review. *Build. Environ.* **2017**, *111*, 123–131. [CrossRef]